ELSEVIER

Sensors and Actuators B 61 (1999) 170–182

SENSORS AND ACTUATORS B CHEMICAL

www.elsevier.nl/locate/sensorb

# Transient response analysis of an electronic nose using multi-exponential models

Ricardo Gutierrez-Osuna [a,*], H. Troy Nagle [b], Susan S. Schiffman [c]

[a] *Computer Science and Engineering Department, Wright State University, Dayton, OH 45435-0001, USA*
[b] *Electrical and Computer Engineering Department, North Carolina State University, Raleigh, NC 27695-7911, USA*
[c] *Department of Psychiatry, Duke University Medical Center, Durham, NC 27712, USA*

Received 10 September 1998; received in revised form 26 August 1999; accepted 26 August 1999

**Abstract**

The purpose of this study is to model the transient response of conductivity-based gas sensors in the context of odor recognition with an electronic nose. Commonly, only the steady-state response of the sensor is used for pattern recognition, ignoring the transient response, which conveys useful discriminatory information. The transient response is modeled as a sum of real exponential functions that represent the different decay processes that occur during sampling of the gas into the sensor chamber and adsorption of the odor compounds onto the sensing element. Four multi-exponential models are reviewed: Gardner transform, multi-exponential transient spectroscopy, Pade-Laplace and Pade-Z transforms. Validation on experimental data from an array of conducting-polymer gas sensors shows that the Pade-Laplace and Pade-Z models have better resolution capabilities than the two spectral transforms. 

*Keywords:* Gardner transform; Multi-exponential transient spectroscopy; Pade-Laplace transform; Pade-Z transform; Electronic nose; Transient response analysis

## 1. Introduction

The objective of this research is to extract information from the transient response of chemical gas sensors for the purpose of identifying volatile compounds with a sensor array. The most common practice for this problem is to use the steady state of the sensors as a feature vector and ignore the transient response, which contains additional discriminatory information [8,20]. Fig. 1 shows the typical response of an array of conducting-polymer gas sensors when exposed to a volatile compound. The exponential nature of the response can be easily observed. It seems that a reasonable way to model these curves would be to fit a sum of exponential functions of the form:

$$f(t) = \sum_{i=1}^{M} G_i e^{-t/\tau_i} \quad (1)$$

Two tasks can be accomplished by modeling the sensor response with Eq. (1). First, a compact representation of the sampled data is obtained: $\{f_k \ldots\} \rightarrow \{G_i\}$. Second, the model parameters may be used as a feature vector $\{G_i, \tau_i, i = 1, \ldots M\}$ for classification purposes. Although conceptually easy, the task of modeling a curve with a set of exponential functions with real exponents is ill-conditioned. Unlike the familiar sinusoidal functions used in Fourier analysis, exponential functions are not an orthogonal base of the real axis. Therefore, the problem of determining the coefficients $\{G_i, \tau_i, i = 1, \ldots M\}$ from finite-time and finite-precision samples of the transient will not have a unique solution. An additional problem is the determination of $M$, the number of exponential components that should be used in the fit. This issue has been known for over forty years, when Lanczos [9] demonstrated that three-exponential curves with similar time constants could be fitted accurately with two-exponential models having significantly different amplitudes and time constants.

## 2. Related work

### 2.1. Classification of methods

The task of fitting a model like Eq. (1) is shared by a variety of disciplines in science [13]: gas relaxation kinet-

* Corresponding author. Tel.: +1-937-775-5120; fax: +1-937-775-5133; e-mail: rgutier@cs.wright.edu

0925-4005/99/$ - see front matter 
PII: S0925-4005(99)00290-7

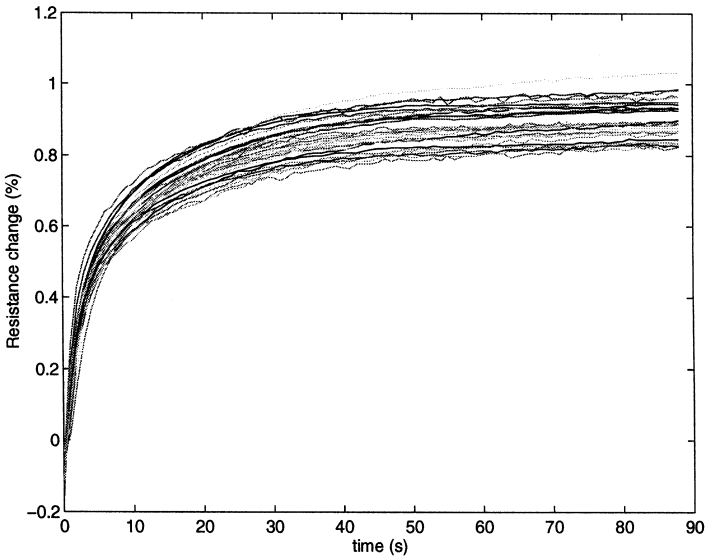


Fig. 1. Typical response of an array of 32 conducting-polymer gas sensors.

ics, fluorescence and radioactivity, sedimentation, nuclear magnetic resonance, etc. A number of methods have been developed, which can be grouped in three classes [3].

(a) Stepwise or exhaustion: These methods extract the different exponential components sequentially, as in the case of ''curve peeling'' [18]. They can be considered as non-global since each component is extracted independently from the rest.

(b) Global approximation or least squares: These methods attempt to approximate the entire curve with a known number of exponential components by minimizing a measure of the fit. Therefore, they are not aimed at component detection.

(c) Global detection or integral transform: These methods share similarities with (a) and (b). Like (a) they are true component detectors. Like (b) they are global since all the model parameters are used simultaneously. A variety of these methods have been proposed, most of them based on classical transformations such as the Fourier transform [6], the Laplace transform [21] and the Z-transform [19].

An alternative classification scheme for multi-exponential methods, based on the characteristics of the resulting models, will be adopted for this study.

(A) Spectral: These methods attempt to recover the spectrum of time constants $G(\tau)$:

$$f(t) = \int_0^\infty G(\tau)\mathrm{e}^{-t/\tau}\mathrm{d}\tau \qquad (2)$$

Spectral methods have several advantages [13]:

- Unlike in (b), the number of exponential terms does not need to be known a priori. The individual exponential components will be detected as peaks in the spectrum.
- Unlike in (a), they are global methods, since all the components are obtained simultaneously in the spectrum.
- Unlike all of the previous methods, the width of the peaks can be used to infer the resolution power of the spectrum. As an example, wider peaks suggest that two or more exponential components with similar time constants have not been resolved.

(B) Non-spectral. These methods attempt to recover the finite set of exponential components $\{G_i,\tau_i,i=1,\ldots M\}$, as in Eq. (1). This class encompasses most of the methods in (a), (b) and (c). The advantage of these methods is that they perform data compression and feature extraction simultaneously, whereas the spectral methods return a distribution that needs to be analyzed afterwards.

Four modeling methods will be analyzed in this study: [1] Gardner transform and multi-exponential transient spectroscopy (METS) from the group of spectral techniques, and Pade-laplace and Pade-Z from the non-spectral family of methods. All four techniques can be regarded as global detection or integral transform methods.

### 2.2. Survey

The Gardner transform [6] was introduced forty years ago, when the ''curve peeling'' method was common practice. The method, based on the Fourier transform, did not become popular at the time due to the lack of computational resources. Schlesinger [14] adapted the Gardner transform to the FFT, but his method lacked a good filtering technique to eliminate side ripples in the spectrum caused by the FFT and noise. For this reason, his implementation was unable to detect the components of a four-

[1] A nonlinear least-squares method based on the Levenberg-Marquardt optimization procedure was also elevated. Its performance on the synthetic multi-exponential curves of Section 4 was very poor and, for this reason, was not included in this report.

exponential synthetic curve. His study was later revisited by Smith and Cohn-Sfetcu [15], who improved the recovery of the spectrum by applying a low-pass Gaussian filter before the de-convolution step of the transform. In a later article, Smith et al. [17] performed a comparison between the Gardner transform and two other spectral techniques: the orthonormal exponential transform and the inverse Laplace transform. The Gardner transform outperformed these two methods, both of which displayed substantial limitations. The orthonormal exponential transform could not handle non-integer time constants, whereas the inverse Laplace transform was unable to recover a simple exponential.

Multi-exponential transient spectroscopy (METS) is a recent method based on multiple differentiation of the experimental curve in logarithmic scale. The theoretical derivation and numerical implementation of METS were presented in Ref. [13]. METS was revisited in Ref. [12] along with some filtering techniques. Finally, Di Natale et al. [5] performed a comparison between METS, auto-regressive models (AR) and moving average models (MA). METS outperformed AR and MA in recovering the time constants and predicting the steady-state value of the sensor.

A substantial body of literature exists on the Pade-Laplace method. The seminal article of Yeramian and Claverie [21], published in 1987, was a high-level overview of the method with several numerical examples. In a later article [3], the authors presented a detailed mathematical derivation of the method, and connections to other methods of multi-exponential analysis. The Pade-Laplace method has been applied to a variety of problems. Bajzer et al. [1] used the Pade-Laplace transform to analyze fluorescence intensity decays. Their contribution was threefold. First, they extended the method to the frequency domain. Second, they proposed a graphical representation, the lifetime-fraction scattergram, to find clusters of poles and residues in the Pade approximants of different order. Third, they presented a heuristic for the determination of an optimal value of $s_0$, the expansion value for the Taylor series of the Laplace transform. Clayden [4] used the Pade-Laplace method on nuclear magnetic resonance (NMR) relaxation decay curves. He concluded that Pade-Laplace was unable to recover three-exponential curves with similar time constants (the ratios were 1:1.8:32.4), and that it performed similarly to nonlinear least squares. Bowers et al. [2] applied Pade-Laplace to electric birefringence decays. They reviewed the heuristic search for $s_0$ of Bajzer et al., concluding that it did not lead to the optimal value. They also performed a comparison between Pade-Laplace and CONTIN, a constrained regularization method, and concluded that Pade-Laplace was more robust to high-frequency noise, but was heavily affected by baseline offsets.

The Pade-Z transform has had an interesting history. Although the term was coined by Yeramian and Claverie, it has been know for over 200 years. Its original ancestor is the Prony method, which was reformulated by Weiss and McDonough [19] using the Z-transform. The Pade-Z method is more appropriate for time-series with a few samples and, unlike the Pade-Laplace method, does not suffer from numerical integration problems [22]. To the best of our knowledge, the only published implementation of the Pade-Z method other than the original one of Yeramian and Claverie is in the article of Ivanov et al. [7].

## 3. Mathematical derivation

### 3.1. Gardner transform

A brief overview of the mathematical derivation of the Gardner Transform follows. For details, the reader is referred to Ref. [6]. Assume an experimental function $f(t)$ such that:

$$f(t) = \sum_{i=1}^{M} G_i e^{-\lambda_i t} \tag{3}$$

Using the definition of the spectrum $g(\lambda)$, Eq. (3) can be rewritten as:

$$f(t) = \int_0^{\infty} g(\lambda) e^{-\lambda t} d\lambda = \int_0^{\infty} \left( \sum_{i=1}^{M} G_i \delta(\lambda - \lambda_i) \right) e^{-\lambda t} d\lambda \tag{4}$$

Performing the change of variables $\lambda = e^{-y}$, $t = e^{x}$:

$$f(e^x) = \int_{-\infty}^{+\infty} \exp[-e^{x-y}] g(e^{-y}) e^{-y} dy \tag{5}$$

The Fourier transform of $e^x f(e^x)$ can be expressed as:

$$\begin{aligned} F(\mu) &= \frac{1}{\sqrt{2\pi}} \int_{-\infty}^{+\infty} e^x f(e^x) e^{i\mu x} dx \\ &= \frac{1}{\sqrt{2\pi}} \int_{-\infty}^{+\infty} \left\{ \int_{-\infty}^{+\infty} \exp[-e^{x-y}] e^{x-y} g(e^{-y}) dy \right\} \\ &\quad \times e^{i\mu x} dx \end{aligned} \tag{6}$$

Using another change of variables $s = x - y$, $F(\mu)$ becomes:

$$F(\mu) = \frac{1}{\sqrt{2\pi}} \int_{-\infty}^{+\infty} g(e^{-y}) e^{i\mu y} \int_{-\infty}^{+\infty} \exp[-e^s] e^s e^{i\mu s} ds \tag{7}$$

Merging expressions (6) and (7), and calling $K(\mu) = \int_{-\infty}^{+\infty} \exp[-e^s] e^s e^{i\mu x} ds$:

$$\begin{aligned} G(\mu) &= \int_{-\infty}^{+\infty} g(e^{-y}) e^{i\mu y} dx = \frac{F(\mu)}{K(\mu)} \\ &= \frac{\int_{-\infty}^{+\infty} e^x f(e^x) e^{i\mu x} dx}{\int_{-\infty}^{+\infty} \exp[-e^s] e^s e^{i\mu x} ds} \end{aligned} \tag{8}$$

Table 1
Time constants and amplitudes of the synthetic signals

| Case 1: $G_i = G_j$ | | Case 2: $G_i\tau_i = K$ | |
|---|---|---|---|
| $G_i$ | $\tau_i$ | $G_i$ | $\tau_i$ |
| 10 | 5 | 1000 | 5 |
| 10 | 22.22 | 225 | 22.22 |
| −10 | 50 | −100 | 50 |
| 10 | 111.11 | 45 | 111.11 |
| 10 | 500 | 10 | 500 |

So the Fourier transform $G(\mu)$ of the spectrum $g(e^{-y})$ can be computed as the ratio of $F(\mu)$ and $K(\mu)$, the Fourier Transforms of the functions $e^x f(e^x)$ and $\exp(-e^s)e^s$, respectively. The inverse Fourier transform of $G(\mu)$ is related to the spectrum $g(\lambda)$ by:

$$g(e^{-y})dy = \frac{g(\lambda)}{\lambda}d\lambda \tag{9}$$

An important remark must be made at this point. The Gardner transform cannot entirely recover the exponential spectrum $g(\lambda)$. Notice that $g(\lambda)$ and $\lambda$ are coupled in Eq. (9). This condition biases the Gardner transform towards multi-exponential curves for which the product of amplitude and time constant is similar for all the exponential components.

The two convolutions and the de-convolution of Eq. (8) are implemented using the FFT. The success of the numerical solution is limited by the fact that:

1. The function $g(e^{-y})$ is not well-behaved.
2. The experimental function $f(t)$ must be sampled with a logarithmic time scale, as required by the FFT of $e^x f(e^x)$. If $f(t)$ is sampled at constant time intervals, an interpolation step must be performed, [2] which can be difficult if $f(t)$ is noisy.
3. The continuous Fourier transform is approximated with its discrete version.
4. The a-periodical convolution of the Fourier Transform is replaced by the circular convolution of the FFT.
5. The de-convolution process favors high-frequency components and, therefore, experimental noise.

As suggested in Ref. [15], the implementation used in this study uses a low-pass Gaussian filter prior to the de-convolution step. This is simply equivalent to multiplying $G(\mu)$ by $-e^{\mu^2/\mu_D^2}$ right before performing the Inverse FFT. The dispersion parameter $\mu_D$ must be tuned to the particular experimental conditions. The smaller the value of $\mu_D$, the better the noise-to-signal ratio of the spectrum, at the price of a lower spectrum resolution.

[2] The implementation used in this article uses polynomial and cubic spline interpolation.

### 3.2. Multi-exponential transient spectroscopy (METS)

METS [13] is based on a multiple differentiation of the experimental function in logarithmic scale. By definition, the first order signal $METS_1$ is:

$$\begin{aligned} METS_1(t) &= \frac{df(t)}{dLnt} = \frac{d}{dLnt}\left[\int_0^\infty G(\tau)e^{-t/\tau}d\tau\right] \\ &= \frac{d}{dt}\left[\int_0^\infty G(\tau)e^{-t/\tau}d\tau\right]\frac{dt}{dLnt} \\ &= -\int_0^\infty \left(\frac{t}{\tau}\right)G(\tau)e^{-t/\tau}d\tau \end{aligned} \tag{10}$$

Performing the change of variables $y = Ln(t)$, $z = Ln(\tau)$ and substituting in Eq. (10):

$$METS_1(t) = \int_{-\infty}^{+\infty} \exp(y - z - e^{y-z})G(e^z)e^z dz \tag{11}$$

Renaming $h(y) = \exp(y - e^y)$ and $TG(z) = e^z G(e^z)$ then:

$$\begin{aligned} METS_1(y) &= -\int_{-\infty}^{+\infty} h(y-z)TG(z)dz \\ &= -h(y)^* TG(z) \end{aligned} \tag{12}$$

If the experimental function has the desired form (1), then $METS_1$ will be the linear combination of the bell-shaped functions $h(y) = \exp(y - e^y)$, which can be thought of as convolution kernels located at $y_i = Ln(\tau_i)$ that multiply the amplitude of the exponential $G_i$.

$$\begin{aligned} f(t) &= \sum_{i=1}^{M} G_i e^{-t/\tau_i} \Rightarrow METS_1(y) \\ &= -\sum_{i-1}^{M} G_i h(y - Ln\tau_i) \end{aligned} \tag{13}$$

Thus $METS_1$ will present peaks at the time constants and the relative amplitude of each peak will be proportional to the amplitude of the exponential component. Replacing the convolution kernel $h(y)$ by the function $h_n(y) = \exp(ny - e^y)$ yields the $n$th-order signal $METS_n$:

$$\begin{aligned} METS_n(y) &= -\int_{-\infty}^{+\infty} h_n(y-z)TG(z)dz \\ &= -h_n(y)^* TG(z) \end{aligned} \tag{14}$$

Differentiation of Eq. (14) yields a useful recursion for the computation of $METS_n$ signals of higher order.

$$\frac{dMETS_n(y)}{dy} = nMETS_n(y) - METS_{n+1}(y) \tag{15}$$

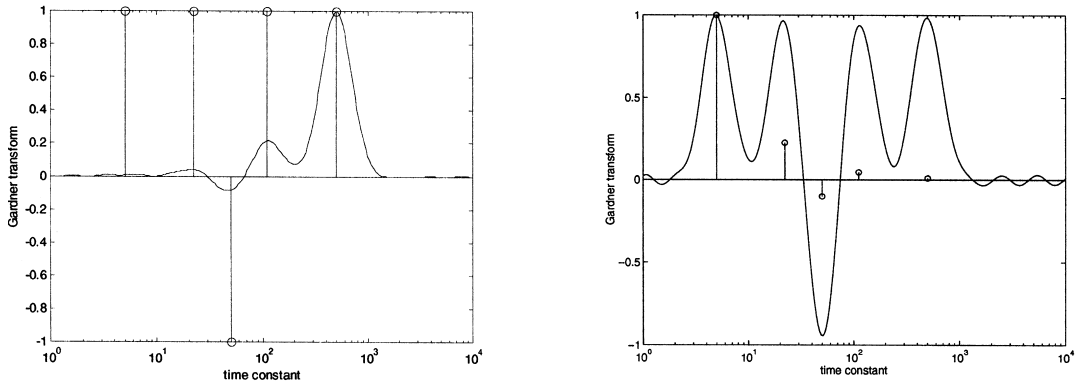


Fig. 2. Gardner transform for synthetic curves: Case 1 (left) and Case 2 (right).

and, similarly, if $f(t) = \sum_{i=1}^{M} G_i e^{-t/\tau_i}$, then:

$$\mathrm{METS}_n(y) = -\sum_{i=1}^{M} G_i h_n(y - Ln\tau_i) \tag{16}$$

The kernels $h_n(y) = \exp(ny - e^y)$ become narrower and more symmetric with increasing order $n$. This can be interpreted as an increase in the resolution power of the transform. An increase in resolution that does not come for free. First, with increasing $n$ the peak of the kernels shifts towards the right on the real axis, distorting the spectrum. Second, since the higher order $\mathrm{METS}_n$ signals are obtained by differentiation, they become very sensitive to high-frequency noise.

The first order signal $\mathrm{METS}_1$ is obtained from the experimental function $f(t)$ by differentiation in logarithmic scale using Eq. (10). This requires logarithmic sampling or interpolation if $f(t)$ is sampled at constant time intervals. Subsequent higher order $\mathrm{METS}_n$ signals are obtained from the recursive expression (15). METS has several advantages over the Gardner transform: (i) METS is computationally cheaper, (ii) it has a trivial implementation and (iii) it allows different degrees of resolution by changing the order of the differentiation.

### 3.3. Pade-Laplace

The Pade-Laplace method [21] is based on the theory of Pade approximants and the Laplace Transform. Assume the same experimental function (3), whose Laplace Transform is:

$$F(s) = \int_0^{\infty} e^{-st} f(t)\,dt = \sum_{i=1}^{M} \frac{G_i}{s - \dfrac{1}{\tau_i}} \tag{17}$$

To obtain the previous analytical expression, from which identification of the individual exponential components is trivial, the Pade-Laplace method proceeds in three steps. First, the Laplace Transform is approximated with a Taylor series at an expansion point $s_0$:

$$\hat{F}(s) = \sum_{j=0}^{K} \frac{1}{j!} \frac{d^j}{ds^j} F(s)|_{s=s_0} (s - s_0)^j \tag{18}$$

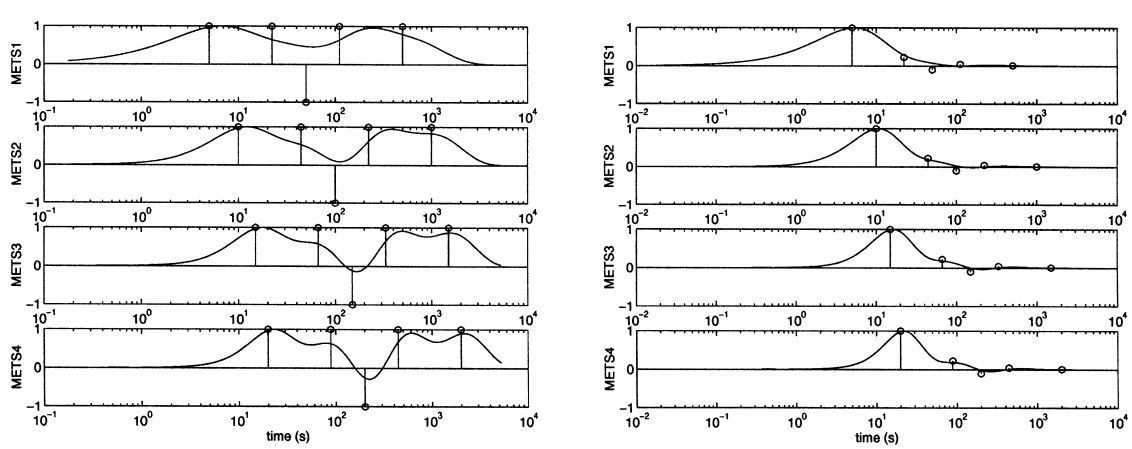


Fig. 3. METS signals for synthetic curves: Case 1 (left) and Case 2 (right).

Table 2
Pade-Laplace results for the first synthetic curve

| # | Stable | Re$\tau_i$ | Im$_{\tau i}$ | ReG$_i$ | ImG$_i$ |
|---|---|---|---|---|---|
| *Poles and residues of the Pade approximant [0 / 1]* | | | | | |
| 1 | | 171.673686 | −0.000000 | 19.257355 | 0.000000 |
| *Poles and residues of the Pade approximant [1 / 2]* | | | | | |
| 1 | | 10.147560 | −0.000000 | 12.453994 | −0.000000 |
| 2 | | 346.123370 | −0.000000 | 14.663474 | 0.000000 |
| *Poles and residues of the Pade approximant [2 / 3]* | | | | | |
| 1 | | 9.236594 | −0.000000 | 12.843732 | 0.000000 |
| 2 | | 328.142697 | −0.000000 | 14.773263 | −0.000000 |
| 3 | | −260.758527 | 0.000000 | 0.073693 | 0.000000 |
| *Poles and residues of the Pade approximant [3 / 4]* | | | | | |
| 1 | | 9.551318 | −0.000000 | 12.824072 | 0.000000 |
| 2 | | 366.264679 | −0.000000 | 14.616748 | 0.000000 |
| 3 | | −6.004231 | 135.151108 | 0.049065 | 0.136904 |
| 4 | | −6.004231 | −135.151108 | 0.049065 | −0.136904 |
| *Poles and residues of the Pade approximant [4 / 5]* | | | | | |
| 1 | | 7.293974 | −0.000000 | 10.359027 | 0.000000 |
| 2 | | 33.333270 | −12.184416 | −0.344979 | −6.342751 |
| 3 | | 33.333270 | 12.184416 | −0.344979 | 6.342751 |
| 4 | | 119.408065 | −0.000000 | 8.470414 | 0.000000 |
| 5 | | 502.942183 | −0.000000 | 9.893369 | 0.000000 |
| *Poles and residues of the Pade approximant [5 / 6]* | | | | | |
| 1 | | 0.084650 | −0.000000 | −35.234956 | −0.000000 |
| 2 | √ | 4.999833 | −0.000000 | 10.000680 | 0.000000 |
| 3 | √ | 22.219952 | −0.000000 | 10.000006 | 0.000000 |
| 4 | √ | 50.000219 | −0.000000 | −10.000148 | −0.000000 |
| 5 | √ | 111.108263 | −0.000000 | 10.000247 | 0.000000 |
| 6 | √ | 500.018237 | −0.000000 | 9.999924 | 0.000000 |
| *Poles and residues of the Pade approximant [6 / 7]* | | | | | |
| 1 | | 0.084650 | −0.000000 | −35.230851 | −0.000000 |
| 2 | √ | 4.999833 | −0.000000 | 9.999515 | 0.000000 |
| 3 | √ | 22.219952 | −0.000000 | 9.998841 | 0.000000 |
| 4 | √ | 50.000219 | −0.000000 | −9.998984 | −0.000000 |
| 5 | √ | 111.108263 | −0.000000 | 9.999082 | 0.000000 |
| 6 | √ | 500.018237 | −0.000000 | 9.998760 | 0.000000 |
| 7 | | −50.000000 | 0.000000 | 0.000000 | 0.000000 |

where

$$\frac{\mathrm{d}^j}{\mathrm{d}s^j}F(s) = \int_0^\infty (-t)^j f(t)\mathrm{e}^{-st}\mathrm{d}t \qquad (19)$$

Second, a Pade approximant is computed for the polynomial expression (18). A Pade approximant $[L/M](s)$ is a rational expression obtained by the division of two polynomials $A_L(s)$ and $B_M(s)$. This approximant [3] has the particular feature that its power series expansion agrees with the Taylor series up to the term $s^{L+M}$.

$$[L/M](s) = \frac{A_L(s)}{B_M(s)} = \frac{a_0 + a_1 s^1 + \ldots + a_L s^L}{b_0 + b_1 s^1 + \ldots + b_M s^M} \qquad (20)$$

Finally, a partial fraction expansion of the Pade approximant (20) yields the time constants and amplitudes from the poles and residues of the expansion, respectively.

The rational expression for the Laplace transform (17) is the ratio of two polynomials with degrees $M$ and $M+1$ in the numerator and denominator, respectively. If the number of exponential components $M$ were known beforehand, only the $[M/M+1]$ approximant would be necessary. But the value of $M$ is generally unknown, forcing the Pade-Laplace method to compute the, $[1/2]$, $[2/3]$, … $[N/N+1]$ Pade approximants and analyze the behavior of their poles. As the order $N$ of the approximant exceeds the true number of exponentials $M$, unstable or ''artificial'' poles will become noticeable, while the true poles will remain stable between consecutive approximants. At that point, the evaluation of Pade approximants can be terminated and the last approximant is returned as a solution.

An important issue in the Pade-Laplace method is the selection of the point $s_0$. For numerical reasons, the method

[3] This article's implementation of the Pade approximants is based on the algorithm presented in Ref. [10].

Table 3
Pade-Laplace results for the second synthetic curve

| # | Stable | Re$\tau_i$ | Im$\tau_i$ | ReG$_i$ | ImG$_i$ |
|---|---|---|---|---|---|
| *Poles and residues of the Pade approximant [1 / 2]* | | | | | |
| 1 | | 10.057084 | −0.000000 | 877.370421 | 0.000000 |
| … | | | | | |
| *Poles and residues of the Pade approximant [5 / 6]* | | | | | |
| 1 | | 0.561255 | −0.000000 | −22.550381 | 0.000000 |
| 2 | √ | 4.997995 | −0.000000 | 1000.486086 | −0.000000 |
| 3 | √ | 22.200775 | −0.000000 | 224.761527 | −0.000000 |
| 4 | √ | 50.150744 | −0.000000 | −100.015250 | 0.000000 |
| 5 | √ | 110.701581 | −0.000000 | 45.315601 | −0.000000 |
| 6 | √ | 498.589394 | −0.000000 | 10.040726 | −0.000000 |
| … | | | | | |

Table 4
Pade-Z results for the first synthetic curve

| # | Stable | Re$\tau_i$ | Im$\tau_i$ | ReG$_i$ | ImG$_i$ |
|---|---|---|---|---|---|
| *Poles and residues of the Pade approximant [1 / 1]* | | | | | |
| 1 | | 160.027037 | 0.000000 | 18.321210 | 0.000000 |
| … | | | | | |
| *Poles and residues of the Pade approximant [5 / 5]* | | | | | |
| 1 | √ | 5.000000 | 0.000000 | 9.801987 | −0.000000 |
| 2 | √ | 22.220034 | 0.000000 | 9.955135 | −0.000000 |
| 3 | √ | 49.999525 | 0.000000 | −9.979746 | −0.000000 |
| 4 | √ | 111.111529 | 0.000000 | 9.990607 | 0.000000 |
| 5 | √ | 499.999994 | 0.000000 | 9.998085 | 0.000000 |
| … | | | | | |

Table 5
Pade-Z results for the second synthetic curve

| # | Stable | Re$\tau_i$ | Im$\tau_i$ | Re$G_i$ | Im$G_i$ |
|---|---|---|---|---|---|
| *Poles and residues of the Pade approximant [1/1]* | | | | | |
| 1 | | 15.643239 | 0.000000 | 481.557784 | 0.000000 |
| … | | | | | |
| *Poles and residues of the Pade approximant [5/5]* | | | | | |
| 1 | √ | 5.000000 | 0.000000 | 998.001969 | 0.000000 |
| 2 | √ | 22.220034 | 0.000000 | 224.900317 | 0.000000 |
| 3 | √ | 49.999524 | 0.000000 | −99.981054 | −0.000000 |
| 4 | √ | 111.111531 | 0.000000 | 44.995390 | 0.000000 |
| 5 | √ | 499.999985 | 0.000000 | 9.999888 | 0.000000 |
| … | | | | | |

will not work for all values of $s_0$. If $s_0$ is too large, the numerical integration in Eq. (19) will truncate the data too early, and the slowest decays will not be identified. If $s_0$ is too small, the integrals in Eq. (19) will not converge in the limited time range provided by the samples of the experimental function. Several iterative heuristics have been presented for the determination of an optimal value of $s_0$ [4,21].

### 3.4. Pade-Z

The Pade-Z transform method is similar to the Pade-Laplace, but it employs the discrete Z transform instead of the continuous Laplace transform. For the experimental function (3), whose sampled version is $f_k = \sum_{i=1}^{M} G_i e^{-kT/\tau_i}$, the Z transform becomes:

$$Z[f_k] = \sum_{i=1}^{M} G_i \frac{z}{z - e^{-T/\tau_i}} \tag{21}$$

Identification of the individual exponential components from Eq. (21) is also trivial. As in the Pade-Laplace method, the Z transform is approximated by its Taylor series expansion at a specific expansion point $z_0$:

$$\hat{F}(z) = \sum_{j=0}^{K} \frac{1}{j!} F^{(n}(z)|_{z=z_0} (z - z_0)^j \tag{22}$$

where:

$$F^{(n}(z) \cong \frac{d^n}{dz^n}\left[\sum_{k=0}^{N-1} f_k z^{-k}\right] = \sum_{k=0}^{N-1} f_k (-1)^n \frac{(k+n-1)!}{(k-1)!} z^{-k-n} \tag{23}$$

Notice that Eq. (23) is approximating the derivative of the analytical Z transform $\sum_{i=1}^{M} G_i (z/z - e^{-T/\tau_i})$ by differentiating the Z transform of the samples $\sum_{k=0}^{N-1} f_k z^{-k}$. Why not use the series $\sum_{k=0}^{N-1} f_k z^{-k}$ itself as the Taylor series expansion and avoid all the burden of Eq. (22) and (23)? It turns out that $\sum_{k=0}^{N-1} f_k z^{-k}$ is the Taylor series expansion of $\sum_{i=1}^{M} G_i (z/z - e^{-T/\tau_i})$ for the choice of $z_0 = \infty$. Numerical experience with the Pade-Laplace method shows that there exists an optimal value of $s_0$, so there exists an optimal value for $z_0$ as well.

The Pade approximants are again computed from the Taylor series expansion. For an analytical Z transform such as Eq. (21), only the $[N/N]$ approximants will be of interest. If the number of exponential components $M$ is known a priori, only the $[M/M]$ Pade approximant needs to be computed. For unknown $M$, a detection procedure similar to the one presented for the Pade-Laplace method can be used.

## 4. Preliminary evaluation on synthetic data

Two noiseless synthetic curves are used to illustrate the capabilities of each method. Each curve contains five

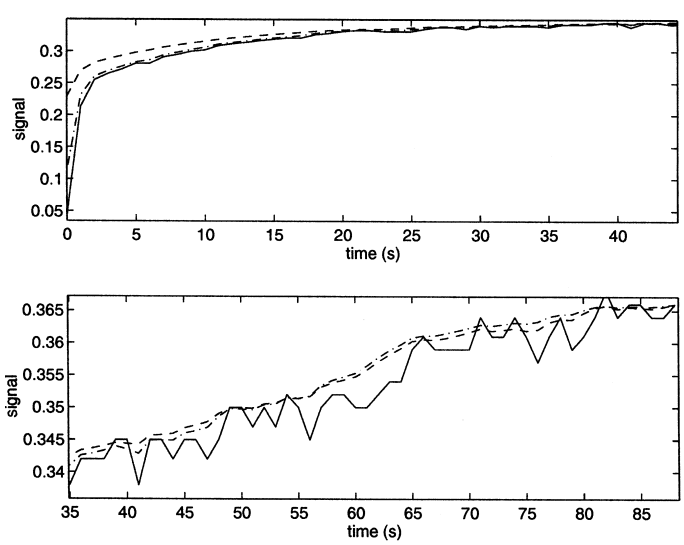


Fig. 4. Low-pass filtering of real data (solid) with an RC filter (dashed) and a decreasing cutoff RC filter (dash-dotted).

exponential components, whose amplitudes and time constants are displayed in Table 1. These cases have been adopted from the literature for comparison purposes. The curves are simulated for 10,000 s with a sampling rate of 0.2 s. In the first case, all components have the same amplitude. In the second case, the product $G_i\tau_i$ is maintained constant for all components, which is the ideal situation for the Gardner transform.

Fig. 2 shows the results of the Gardner transform on the two synthetic curves. The theoretical spectrum, a superposition of delta functions $\sum_{i=1}^{M} G_i\delta(\tau-\tau_i)$, is plotted along with the Gardner Transform for comparison. The curves and theoretical spectrum are normalized for visualization purposes. As anticipated, the Gardner transform performs significantly better on the curve with $G_i\tau_i = K$. The dispersion parameter of the Gaussian low-pass filter was manually set to $\mu_D = \pi/10$.

Fig. 3 shows the results of the METS on the same synthetic curves. The curves are also normalized for visualization purposes. Notice how the resolution increases with the order of the transform. For the $METS_4$, all five components have been extracted.

The same curves were analyzed with the Pade-Laplace routine. Detailed results of the output of the algorithm for the first synthetic exponential are shown in Table 2. The final results for the second synthetic curve are given in Table 3. The expansion point for the Taylor series was manually set to $p_0 = 0.009$. The method finds the five stable exponential components in the $[5/6]$ approximant in both cases.

The final results of the Pade-Z transform are presented in Tables 4 and 5. The method is able to find all the components for both signals, although manual selection of the optimal value $z_0 = 1.01$ was tedious. The five stable exponents are detected at the $[5/5]$ approximant.

## 5. Data filtering

The synthetic multi-exponential data used in the previous section was noiseless, except for the noise introduced by the logarithmic interpolation in METS and the Gardner Transform. This is not the case on the electronic nose experimental data, which needs to be low-pass filtered while preserving the fastest time constants. As shown by Smith and Cohn-Sfetcu [16], the optimal filter for multi-exponential signals is a reverse-time single section RC filter with a time constant much larger than those of the signal components. For a single component decay, the maximum information/noise ratio can be obtained when

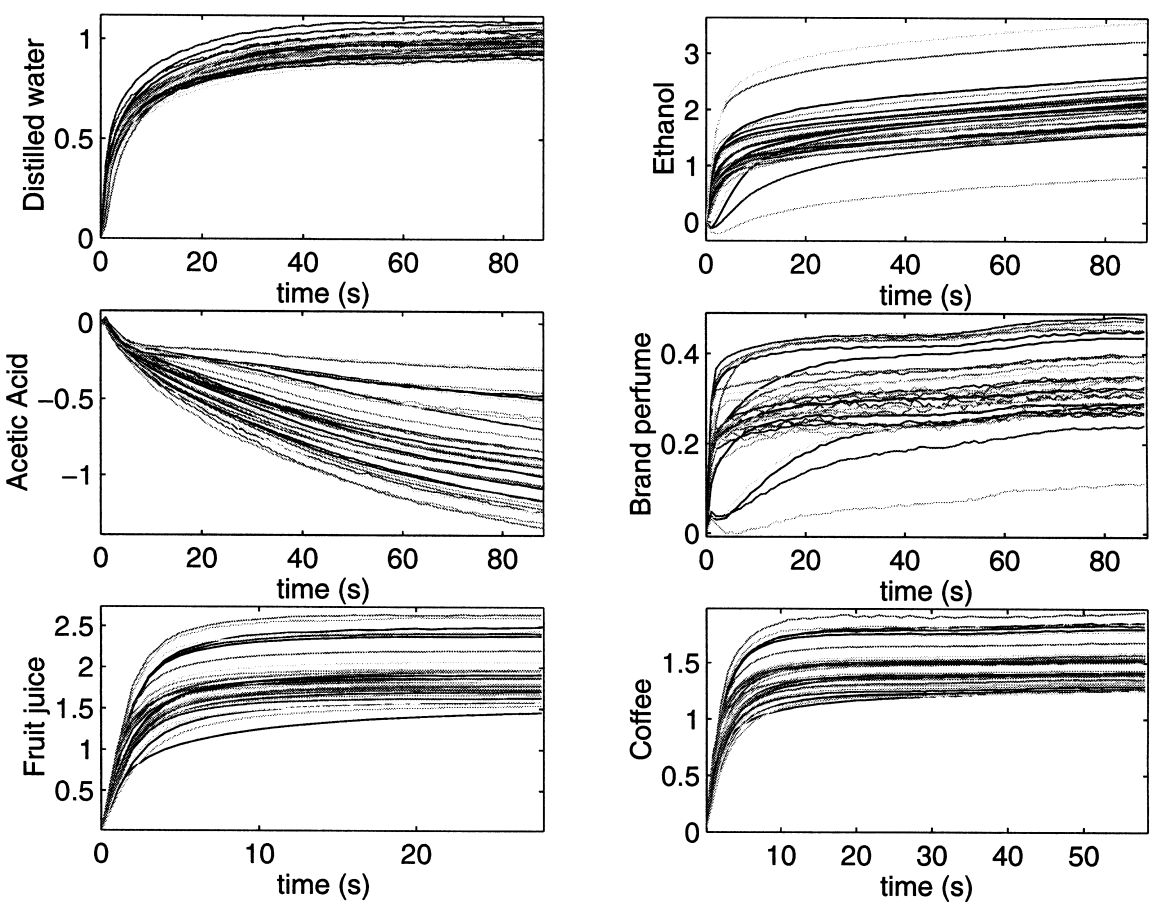


Fig. 5. Database of odor samples.

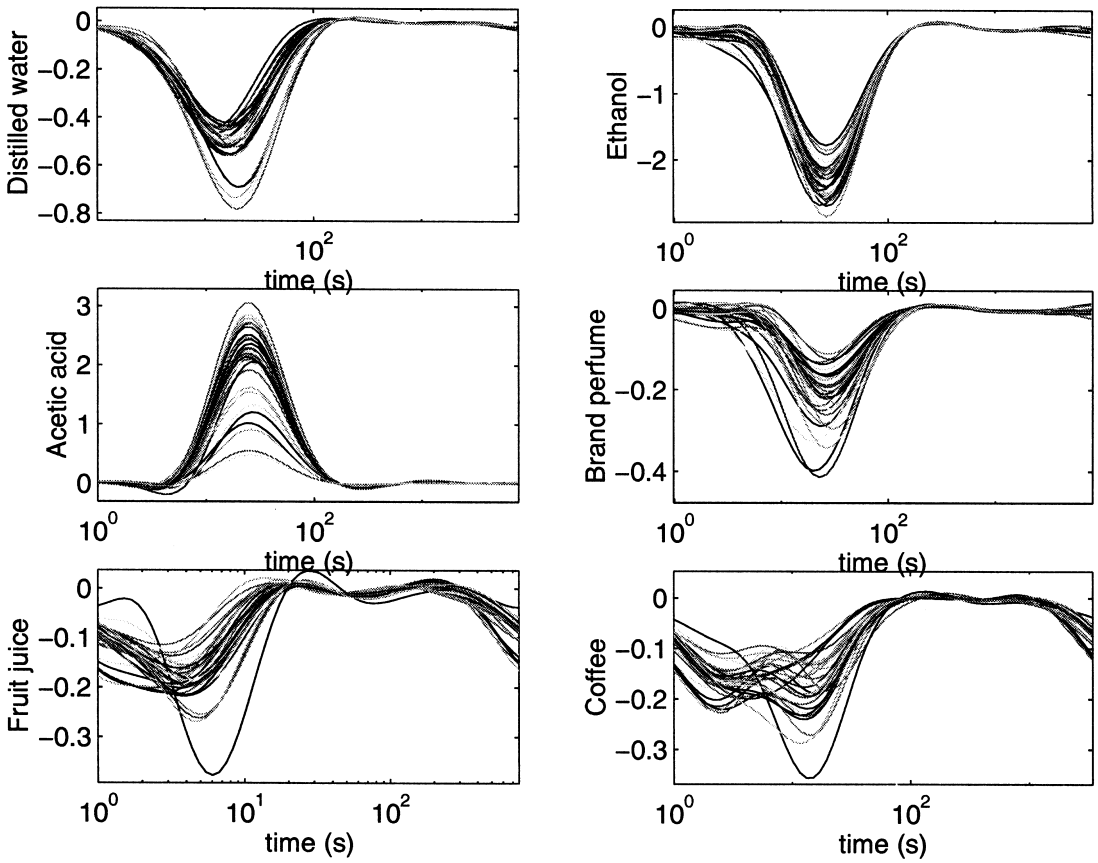


Fig. 6. Gardner transform on real data.

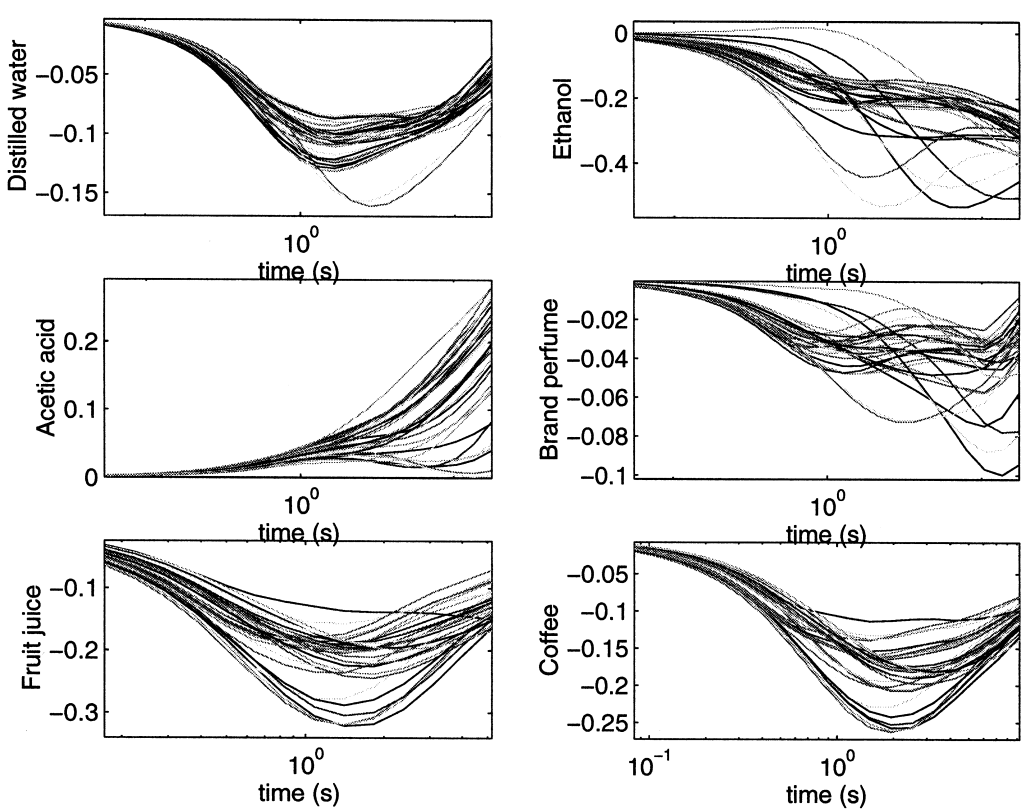


Fig. 7. $METS_1$ signals on real data.

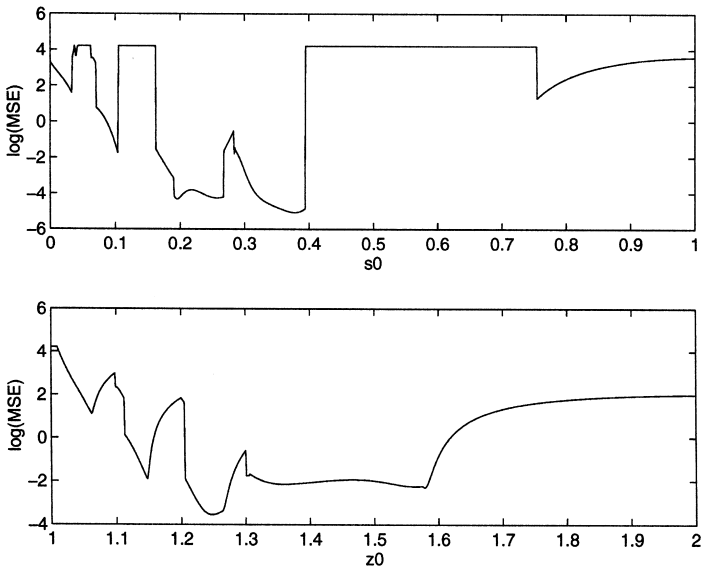


Fig. 8. Search space for $s_0$ and $z_0$.

the filter and the signal have the same time constant. A further improvement can be made if the RC filter is allowed to have a cutoff frequency that decreases with time [11]. This allows the fastest components to be preserved, while eliminating high-frequency noise in the steady-state region. Both constant-cutoff and decreasing-cutoff filters were tested on real data and the results are shown in Fig. 4. The top view shows a pronounced lag in

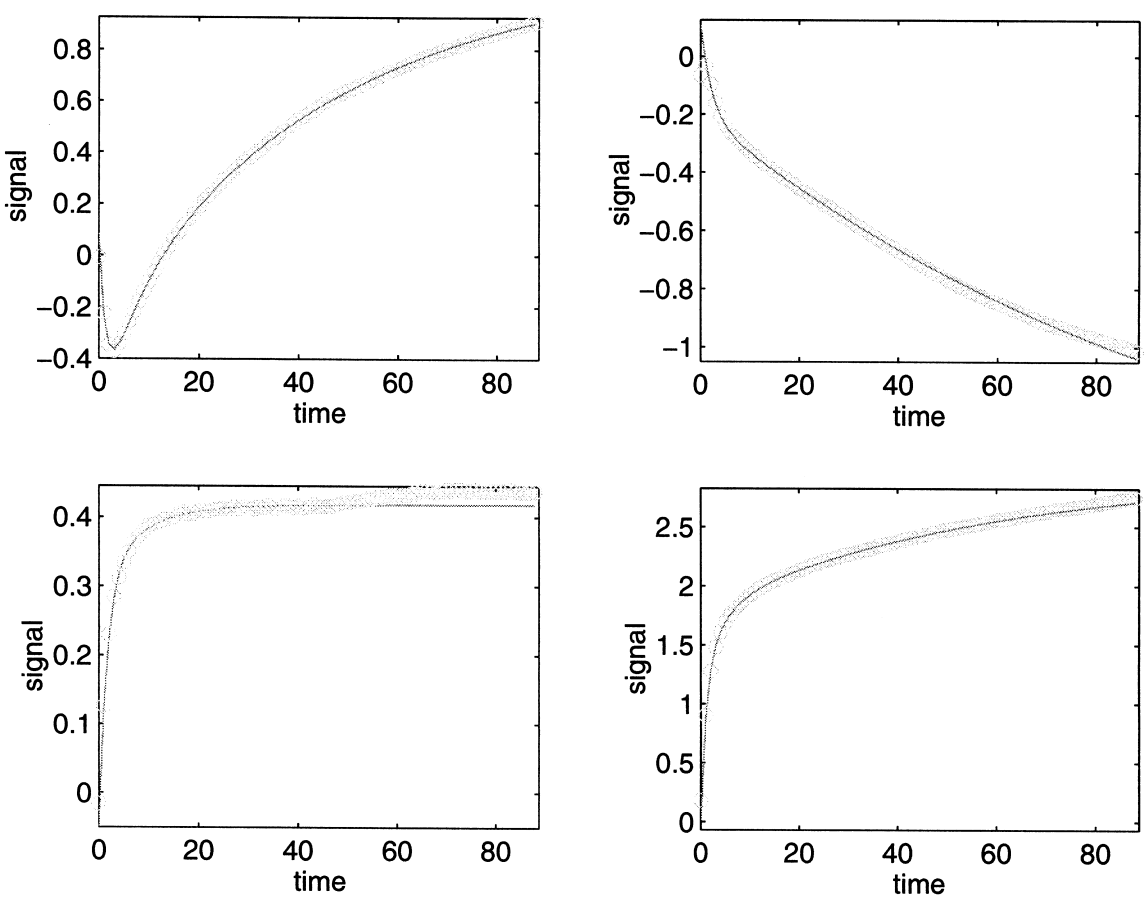


Fig. 9. Example fits between data (circled) and multi-exponential models (solid).

the RC filter. The bottom view zooms on the smoothing effect in the tail of the curve. The advantages of having a decreasing cutoff frequency are very significant.

## 6. Evaluation of real data

The different techniques are now evaluated on data collected from an electronic nose consisting of 32 polymer sensors. Samples from six different odorants: distilled water, ethanol, acetic acid (5% in volume), brand perfume, fruit juice and coffee are used. Fig. 5 shows the first out of three sniffs for each odorant.

### 6.1. Gardner transform

The Gardner Transform is able to extract one time constant from the first five odors, and two time constants from the last odor. The decreased resolution of the transform with respect to synthetic data may be caused by a slow sampling rate of 1 Hz, the reduced number of samples (30–90 typically) and the noise introduced in the logarithmic interpolation step. The dispersion parameter $\mu_D$ was set to 0.01. The 3 dB cutoff frequency of the filter was decreased linearly from to 1 Hz for the first sample to 0.1 Hz for the last sample. The 32 Gardner Transforms for each odor are displayed in Fig. 6.

### 6.2. METS

METS appears to be more sensitive to noise than the Gardner transform. The technique is able to extract one exponential component after the first differentiation ($METS_1$), but the low SNR prevents the use of higher order derivatives. The 3 dB cutoff frequency of the filter was decreased linearly from to 0.2 Hz for the first sample to 0.05 Hz for the last sample. The 32 $METS_1$ signals for each odor are displayed in Fig. 7.

### 6.3. Pade-Laplace

The Pade-Laplace method is more robust to experimental noise than the preceding spectral methods. Its main drawback is the selection of an expansion point $s_0$ for the Taylor series. Although the importance of an appropriate choice for $s_0$ has been corroborated in the literature [1,2,21], there has been little agreement on a general heuristic for the determination of this parameter. For this reason, the implementation used in this study performs an exhaustive search for the optimal value of $s_0$ inside a

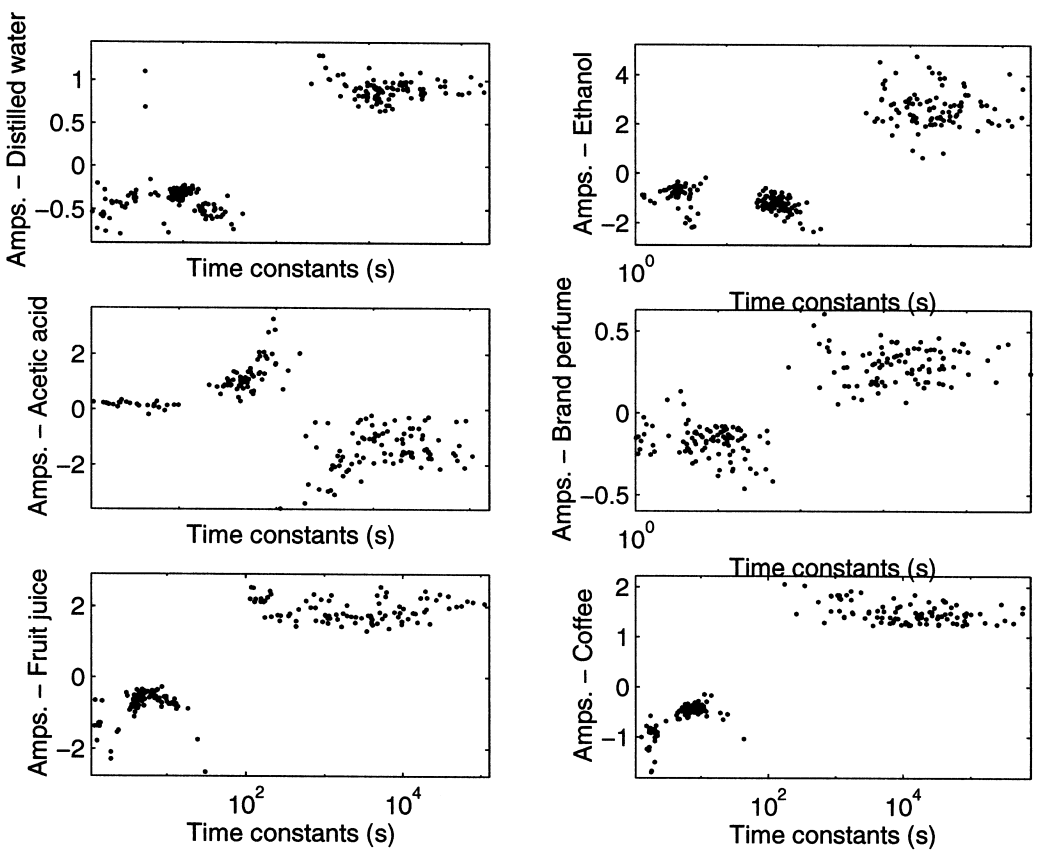


Fig. 10. Lifetime-fraction scattergrams for the Pade-Laplace method.

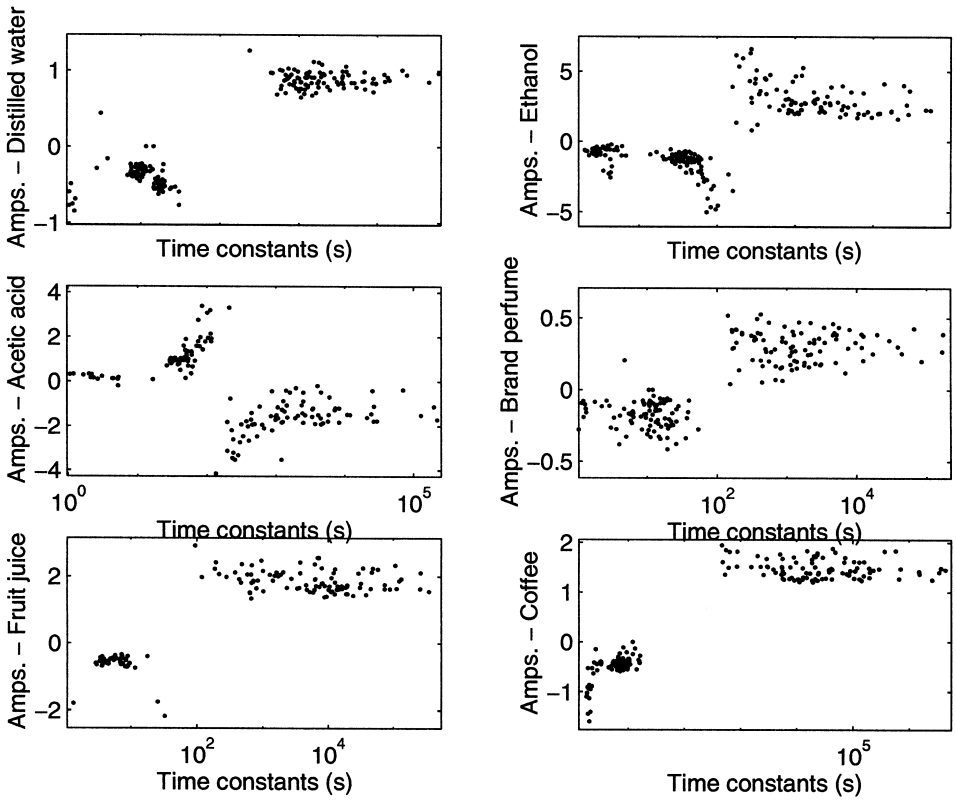


Fig. 11. Lifetime-fraction scattergram for the Pade-Z method.

suitable range manually selected. The optimal $s_0^*$ is chosen as the value that minimizes the sum-squared error (SSE) between the experimental curve and the model:

$$s_0^* = \underset{s_0, M}{\operatorname{argmin}} \left[ \sum_{k=0}^{N-1} \left( f_k - \sum_{i=1}^{M} G_{i,s_0,M} \, \mathrm{e}^{-t/\tau_{i,s_0,M}} \right)^2 \right] \qquad (25)$$

Therefore, for each value of $s_0$ the number of exponentials $M$ is determined by the $[(M-1)/M]$ Pade approximant with minimum SSE, instead of using the detection procedure based on pole stability described in Section 3.3. The search for $s_0$ is performed in several passes with increasing levels of resolution. The first pass uses a large step size over the entire range of $s_0$. Subsequent passes will search the neighborhood of the minimum with smaller step size. The error surface is very irregular, as shown in Fig. 8. This error surface was obtained from one of the distilled water transients.

Although the proposed ad hoc search procedure does not guarantee the optimal value of $s_0$, the resulting curve fits between model and experimental data are visually accurate, as shown in Fig. 9.

Fig. 10 shows the lifetime-fraction scattergrams obtained with the Pade-Laplace method. Each dot represents an exponential component with parameters $(G_i, \tau_i)$. Each scattergram contains the exponential components of 32 sensor transients, and could be used as an odor signature. At least two clusters and, in some cases, three clusters of exponential components can be observed. The clusters with small time constants represent the initial transient of the signal. The cluster to the right of the scattergram represents the steady state, for which $\tau \to \infty$, which explains the spread in the time-constant axis.

### 6.4. Pade-Z

The search for the optimal value of $z_0$ is performed in a similar way as the search for $s_0$ in the Pade-Laplace method. The visual accuracy of the fits is also similar to those of the Pade-Laplace method. The lifetime-fraction scattergrams are shown in Fig. 11.

## 7. Discussion of results

The previous section presented the results of the multi-exponential analysis on experimental data from a 32-element conducting-polymer sensor array. The resolution capabilities of the spectral methods appear to be severely limited by the slow sampling rate, limited number of samples and experimental noise. These methods require logarithmic interpolation of the evenly sampled curves and, therefore, a previous low-pass filtering. Both spectral methods are able to detect one exponential component. The SNR does not allow higher order METS signals to be

used, which would otherwise yield better resolution. The Gardner transform is extremely sensitive to the dispersion parameter $\mu_D$. Neither technique can recover the steady-state value of the curves.

The Pade-Laplace and Pade-Z methods are less sensitive to experimental noise than the spectral techniques and do not require low-pass filtering. Both methods perform similarly in terms of minimum-SSE fit and provide visually accurate curve fits. In most cases, the sensor signals are modeled with two exponential components, although sometimes up to five exponential components are found. These methods can be used for virtually loss-less data compression, with compression ratios as high as 20:1 in most cases.

The remaining question is whether the parameters of the exponential components $(G_i,\tau_i)$ are suitable features for pattern classification or not. Since the exponential functions are non-orthogonal, the parameters might not be repeatable. This issue constitutes the next step of this research. The search for the optimal parameters $s_0$ and $z_0$ has been shown to be non-trivial and deserves a closer look. Finally, the effects of odorant concentration, temperature, humidity and other experimental variables must also be analyzed.

## Acknowledgements

The authors would like to thank Santiago Marco for his useful comments in the implementation of the METS method and low-pass filtering. Edouard Yeramian is also acknowledged for suggesting the Pade-Z transform as a promising method for this study.

## References

[1] Z. Bajzer, A.C. Myers, S.S. Sedarous, F.G. Prendergast, Pade-Laplace method for analysis of fluorescence intensity decay, Biophys. J. 56 (1989) 79–93.
[2] J.S. Bowers, R.K. Prud'Homme, R.S. Farinato, An assessment of the Pade-Laplace method for transient electric birefringence decay analysis, Comput. Chem. 16 (3) (1992) 249–259.
[3] P. Claverie, A. Denis, E. Yeramian, The representation of functions through the combined use of integral transforms and Pade approximants: Pade-Laplace analysis of functions as sum of exponentials, Comput. Phys. Rep. 9 (1989) 247–299.
[4] N.J. Clayden, Pade-Laplace analysis in the fitting of multi-exponential nuclear magnetic resonance relaxation decay curves, J. Chem. Soc. Faraday Trans. 88 (17) (1992) 2481–2486.
[5] C. Di Natale, S. Marco, F. Davide, A. D'Amico, Sensor-array calibration time reduction by dynamic modeling, Sens. Actuators, B 24–25 (1995) 578–583.
[6] D.G. Gardner, J.C. Gardner, G.L. Laush, W.W. Meinke, Method for the analysis of multicomponent exponential decay curves, J. Chem. Phys. 31 (1959) 978–986.
[7] S.A. Ivanov, V.N. Ivanova, V.B. Smirnov, B.Z. Tabin, Z transformation and the Pade approximation in the determination of exponentially attenuated-signal parameters, Opt. Spectrosc. 73 (1992) 150–153.
[8] B.G. Kermani, On using neural networks and genetic algorithms to optimize performance of an electronic nose, PhD Dissertation, Electrical and Computer Engineering Department, North Carolina State Univ., 1995.
[9] C. Lanczos, Applied Analysis, Prentice-Hall, 1956.
[10] I.M. Longman, Computation of the Pade Table, International Journal of Computer Mathematics Section B 3 (1971) 53–64.
[11] S. Marco, Personal communication, 1996.
[12] S. Marco, J. Samitier, J.R. Morante, A novel time-domain method to analyse multicomponent exponential transients, Meas. Sci. Technol. 6 (1995) 135–142.
[13] J. Samitier, J.M. Lopez-Villegas, S. Marco, L. Camara, A. Pardo, O. Ruiz, J.R. Morante, A new method to analyse signal transients in chemical sensors, Sens. Actuators, B 18–19 (1994) 308–312.
[14] J. Schlesinger, Fit to experimental data with exponential functions using the Fast Fourier Transform, Nucl. Instrum. Methods 106 (1973) 503–508.
[15] M.R. Smith, S. Cohn-Sfetcu, Comment on ''Fit to experimental data with exponential functions using the Fast Fourier Transform'', Nucl. Instrum. Methods 114 (1974) 171–173.
[16] M.R. Smith, S. Cohn-Sfetcu, On the design and use of digital filters in certain experimental situations, J. Phys. E: Sci. Instrum. 8 (1975) 515–522.
[17] M.R. Smith, S. Cohn-Sfetcu, H.A. Buckmaster, Decomposition of multicomponent exponential decays by spectral analytic techniques, Technometrics 18 (1976) 467–482.
[18] W.T. Sobol, Analysis of variance for ''component stripping'' decomposition of multiexponential curves, Computer Methods and Programs in Biomedicine 39 (1993) 243–257.
[19] L. Weiss, R.N. McDonough, Prony's method, z-transforms, and Pade Approximation, SIAM Rev. 5 2 (1963) 145–149.
[20] D.M. Wilson, S.P. DeWeerth, Odor discrimination using steady-state and transient characteristics of tin-oxide sensors, Sens. Actuators, B 28 (1995) 123–128.
[21] E. Yeramian, P. Claverie, Analysis of multi-exponential functions without a hypothesis as to the number of components, Nature 326 (1987) 169–174.
[22] E. Yeramian, Personal communication, 1996.

Ricardo Gutierrez-Osuna is Assistant Professor of Computer Science and Engineering at Wright State University, where he is principal investigator of the Pattern Analysis and Machine Intelligence Lab. He received his PhD in Computer Engineering from NC State in 1998.

H. Troy Nagle is Professor of Electrical and Computer Engineering at North Carolina State University. He is principal investigator of the Biomedical Microsensors Laboratory at NC State. He has a Ph.D. in Electrical Engineering from Auburn University and an MD from the University of Miami. He was President of IEEE in 1994.

Susan S. Schiffman is Professor of Psychiatry at the Duke University Medical Center. She earned her PhD in Psychology at Duke University. She is director of the Duke taste and smell laboratory. She is also Editor of the journal Physiology and Behavior.